

# System–Technology Co-Optimization of Bitline Routing and Bonding Pathways in Monolithic 3D DRAM Architectures

Kiseok Lee, Sungwon Cho, Seongkwang Lim, Suman Datta and Shimeng Yu  
 School of Electrical and Computer Engineering, Georgia Institute of Technology, Atlanta, Georgia, USA  
 Email: [shimeng.yu@ece.gatech.edu](mailto:shimeng.yu@ece.gatech.edu)

**Abstract**—3D DRAM has emerged as a promising approach for continued density scaling, but its viability is limited by routing and hybrid bonding constraints to periphery, which may degrade sensing margin, latency, and array efficiency. With device characteristics and array parasitics extracted from TCAD, SPICE simulations are performed with peri logic in a CMOS-Bonded-Array (CBA). The analysis shows that the bitline strap architecture with amorphous oxide semiconductor (AOS) selectors is essential to manage routing congestion and parasitics. The optimized design achieves a bit density of 2.6 Gb/mm<sup>2</sup> (137 layers with Si access transistors or 87 layers with AOS), representing ~6× density scaling over D1b 2D DRAM. The design further demonstrates a nominal row cycle time (tRC) of 10.5 ns, compared to 21.3 ns in D1b, and a 60% reduction in read/write energy.

## I. INTRODUCTION

3D DRAM is key to sustaining density scaling beyond 4F<sup>2</sup> [1]. Recent works prototyped this technology and analysis so far focused on the bit cell and mat (sub-array) level with discussions on access transistor characteristics and tradeoffs between vertical BL and vertical WL [1-6]. Even VBL is preferred, the vertical extension of BLs and the stacking of WLs create severe routing congestion, increased parasitics, and vulnerability to disturb mechanisms such as floating-body effects (FBE) and row-hammering (RH) [7, 8]. To our best knowledge, the analysis beyond the mat-level is lacking for 3D DRAM, while the employment of hybrid bonding introduces new challenges with global routing parasitics and peripheral circuit placement [7]. This study focuses on the

architectural co-optimization that was missing in prior works (Table I), specifically targeting BL routing topologies and CMOS-Bonded-Array (CBA) integration.

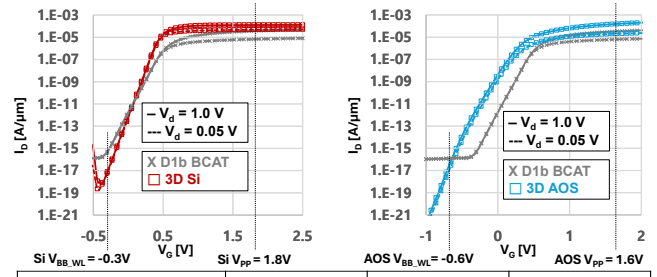
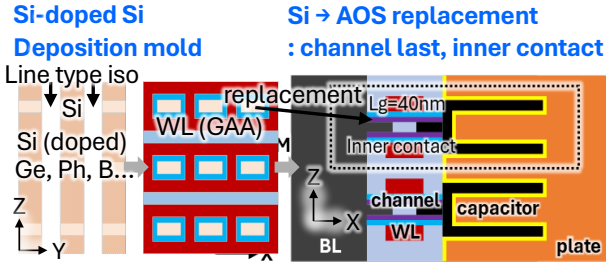
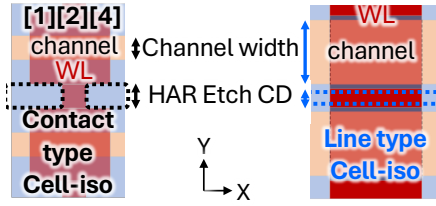
## II. METHODS AND RESULTS

We performed TCAD parasitic extraction and access transistor modeling of Si and amorphous oxide semiconductor (AOS) channel cell architectures, with the AOS model calibrated against the low-leakage W-doped In<sub>2</sub>O<sub>3</sub> (IWO) double gate transistor [9]. The storage node capacitance (Cs) was unified at 4 fF, matching the D1b [10] estimate. The optimal cell configuration was selected; dimensions, extracted characteristics and parasitics are summarized in Fig. 1. The proposed cell architecture features line-type cell isolation (iso) and Si deposition-based mold strategy. Two distinct iso methods are evaluated: Contact-type iso [2, 4] utilizes contact-etch for bilateral WL patterning followed by isotropic Si etching to complete cell iso. However, the lateral recess typically increases the Y-pitch or constricts the channel width (40nm). Following a refined design, line-type iso [7] initiates with a line-etching process and proceeds with full gate wrapping around the Si channel. This configuration minimizes Y-pitch (100nm) while achieving a wider channel width (70 nm). Furthermore, Si deposition-based mold (with channel last and inner contact) for AOS is adopted to effectively reduce the iso-etch pitch [7]. This is enabled by the ease of Si etching compared to SiO<sub>2</sub> and Si<sub>3</sub>N<sub>4</sub>, facilitating more aggressive scaling. BL routing is the dominant factor limiting sense margin and array efficiency.

TABLE I  
 Comprehensive benchmarking of 1T1C 3D DRAM technologies: A multi-level comparison of "This Work" with state-of-the-art implementations from cell and array to architecture and system performance metrics.

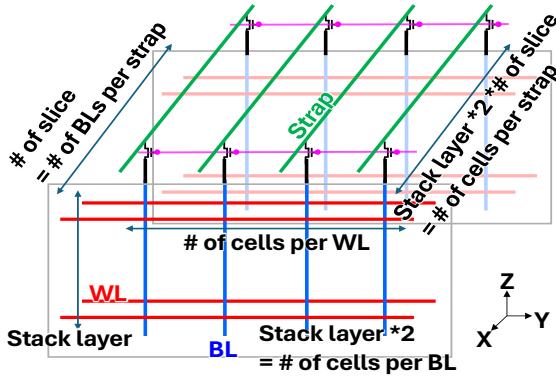
	1T1C 3D DRAM	Samsung VLSI 23 [1]	SK Hynix VLSI 24 [2]	CAS,SAMT IEDM 24 [3]	imec VLSI 25 [4] Imec IEDM 25 [5]	Kioxia IEDM 25 [6]	This Work (What is new?)
Cell	Cell structure	double gate	double gate contact type isolation	P-CAA Isolated channel	GAA contact type isolation	GAA separated WL / gate	GAA line type isolation
	Channel material (mold)	epitaxial Si (Si-SiGe)	epitaxial Si (Si-SiGe)	AOS (TiN-SiO <sub>2</sub> )	epitaxial Si (Si-SiGe)	AOS (SiO <sub>2</sub> -Si <sub>3</sub> N <sub>4</sub> )	epitaxial Si (Si-SiGe) & AOS (Si deposition)
	Access Tr. analysis	experiment + TCAD	experiment	experiment	experiment + TCAD	experiment	TCAD
Array	Array direction	VBL vs. HBL	VBL	HBL	VBL	VBL	VBL
	Array characteristics	6 tier demonstration (no quantitative result)	5 tier demonstration (no quantitative result)	4 tier demonstration (no quantitative result)	3 tier demonstration (no quantitative result)	8 tier demonstration (no quantitative result)	TCAD mini array → full array estimation
	Vulnerability	simple mention : FBE	experiment : FBE	experiment : BTI, endurance, retention	experiment : FBE	experiment : BTI, endurance, retention	TCAD : FBE + RH
Architecture & System	Array organization WL/BL routing to CMOS CMOS formation	simple mention : HCB CBA	experiment : HCB CBA	simple mention : BL selector, strap	none	simple mention : BL/WL selector,strap	HCB CBA : BL/WL selector, strap layout & quantitative analysis (TCAD+SPICE)
	Bit density	none	simple mention (a.u.)	D0a ~72L	D0a 100L, D0b 150L, D0c 200L	simple mention (a.u.)	Dof 2.6Gb/mm <sup>2</sup> : 137L (Si), 87L (AOS)
	Sense margin	none	initial ΔVBL	initial ΔVBL	none	initial ΔVBL (a.u.)	full SWD+BLSA circuit (SPICE, compact model)
	Latency (timing)	none	none	simple mention (a.u.)	none	none	analytical estimation
Energy efficiency	none	none	none	none	none	simple mention (a.u.)	analytical estimation

(a) Proposed cell architecture



VBL, CBA, selector	2D (D1b [11])	3D (Si)	3D (AOS)	
Access transistor	BCAT	GAA line type cell isolation		
Channel	c-Si	Epitaxial Si	IWO	
Dimension	X / Lg [nm]	32.6 / 120	349 / 100	238 / 40
	Y / W [nm]	37.6 / 11.7	100 / 70	100 / 70
	Z [nm]	-	70	80
# of Cells per BL / WL	1280 / 1024	#of layer*2 / 1024	#of layer*2 / 1024	
Cs [fF]	4			
C <sub>BL</sub> per 1 layer [fF]	25.0	0.0815	0.128	
R <sub>BL</sub> per 1 layer [kΩ]	49.6	0.292 (N+ p-Si)	0.0167 (TiN/W)	
C <sub>WL</sub> [fF] / R <sub>WL</sub> [kΩ]	30.0 / 81.2	96.3 / 8.1	94.4 / 19.9	
Parasitic C <sub>WL</sub> [fF]	16.2	42.0	33.2	
I <sub>on</sub> [μA] / I <sub>off</sub> [fA]	2.44 / 0.2	9.03 / 0.02	10.4 / 0.02	
V <sub>th</sub> / V <sub>pp</sub> [V]	0.43 / 2.5	0.30 / 1.8	0.20 / 1.6	
V <sub>BB,WL</sub> / V <sub>BB</sub> [V]	-0.3 / -0.6	-0.3 / -	-0.6 / -	

(b) Array organization concept



(c) TCAD simulation

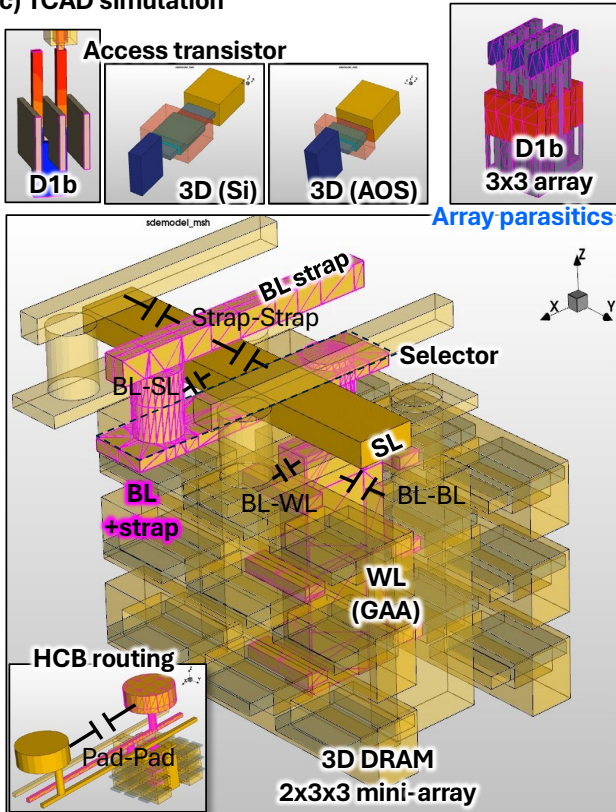


Fig. 1. Geometric and electrical characteristics of baseline D1b [10] and proposed ITIC 3D DRAM (a) proposed cell architecture and integration strategy, (b) array organization concept, (c) multi-scale TCAD simulation (access transistor, array, routing) and results.

We evaluated four distinct routing schemes: (a) Direct BLSA connection, (b) BL strapping, (c) Core MUX, and (d) BL Selector + Strap (Fig. 2). While schemes (a) and (c) offer the lowest delay, they demand a prohibitively tight hybrid Cu bonding (HCB) pitch of 0.26 μm (Si) and 0.22 μm (AOS). Simple strapping (b) relaxes pitch requirements but substantially increases BL parasitic capacitance (CBL), thereby degrading the sense margin. The proposed solution is the "BL Selector + Strap".

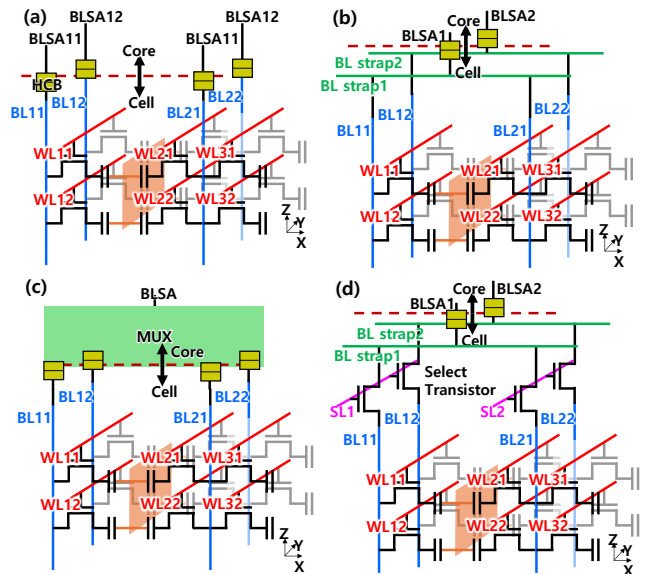


Fig. 2. Schematic comparison of four BL routing architectures. (a) Direct BLSA connection, (b) BL strapping, (c) Core MUX, and (d) BL Selector + Strap.

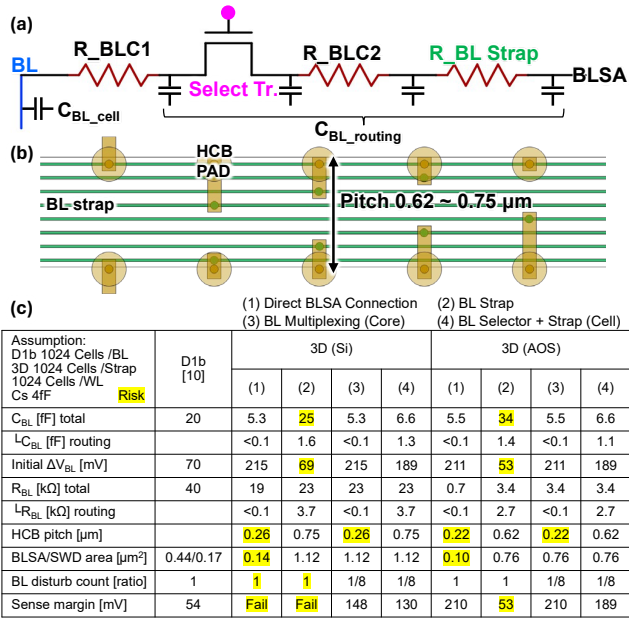


Fig. 3. (a) equivalent circuit, (b) layout of BL strap and HCB routing and (c) comprehensive comparison of BL routing schemes.

As shown in Fig.3, this configuration isolates unselected BLs, reducing effective CBL to 6.6 fF (w/ bonding parasitics) (vs. 20 fF for D1b) and improving the sense margin to 130 mV (Si) and 189 mV (AOS) (vs. 54 mV for D1b). Furthermore, the select transistor enables the inactive BL to float at a refresh potential, effectively mitigating the FBE and off-state leakage by decoupling the cell from the global BL. This strategy also accommodates a relaxed HCB pitch of 0.75  $\mu$ m (Si) and 0.62  $\mu$ m (AOS), which is well within the manufacturable window for W2W HCB, while allowing for a larger BLSA area of 1.12  $\mu$ m<sup>2</sup> (Si), 0.76  $\mu$ m<sup>2</sup> (AOS) compared to D1b (0.44  $\mu$ m<sup>2</sup>).

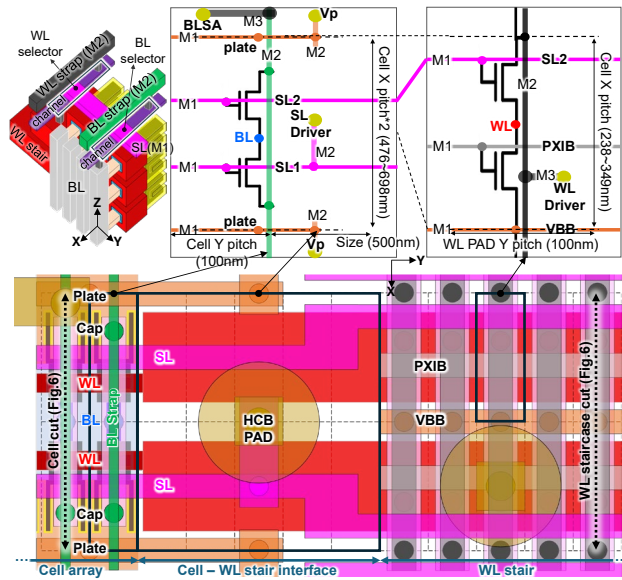


Fig. 4. Layout of selector, WL driver, SL driver and Vp routing.

The physical implementation of this architecture employs a CBA, where the periphery is vertically bonded over the cell array (Fig. 4-5). As detailed in the layout (Fig. 4), the design utilizes a metal stack (M1-M3) to route select lines (SLs) and WL to their drivers within the tight cell pitch, ensuring direct vertical connectivity. The layout (Fig.5) integrates 16 WLs

and 8 BLs per strap, routing them to drivers and BL sense amplifiers (BLSA) located on the overlying CMOS wafer. This vertical integration effectively eliminates the long lateral routing bottlenecks inherent to 2D designs.

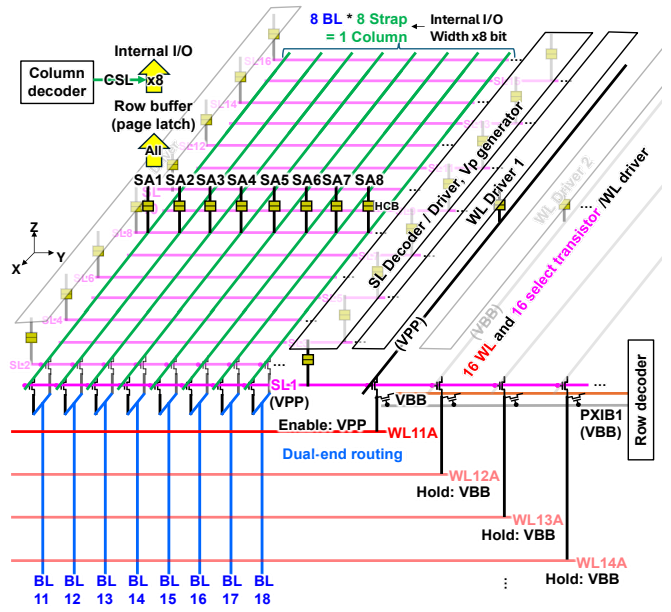


Fig. 5. WL and BL routing, SL/WL driver, BLSA and data path.

As shown in Fig. 6, select transistors are integrated on top of the cell to alleviate routing congestion. To ensure high drivability within tight spatial constraints, Indium-Gallium-Oxide (IGO [11]) was adopted for its performance and BEOL compatibility. The IGO selector can achieve  $I_{on} > 50 \mu$ A @2V ( $W/L = 70 \text{ nm} / 50 \text{ nm}$ ) and a near-ideal 60 mV/dec SS. Such a high-performance device is critical for 16 WL and 8 BL multiplexing schemes, ensuring efficient signal delivery while maintaining a compact footprint.

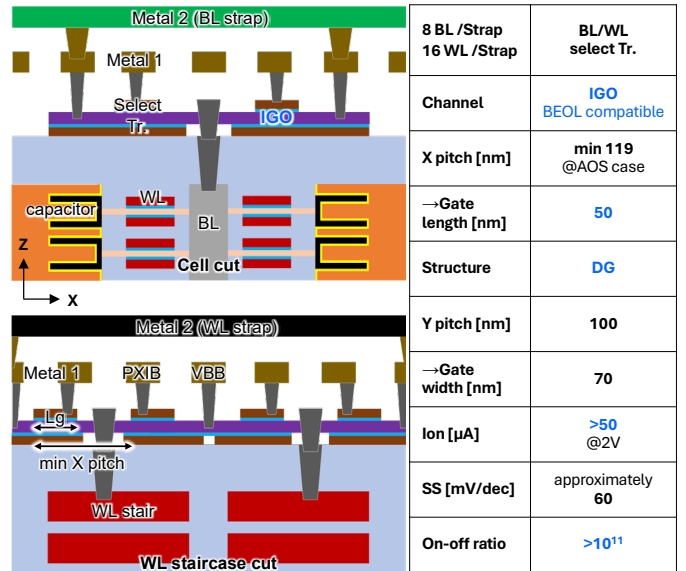


Fig. 6. Cross-section view and performance benchmark of the proposed IGO-based select transistor.

Fig. 7 outlines SPICE circuit topology and operating conditions; notably, the 3D architecture operates at reduced WL overdrive voltages ( $V_{PP}$ : 1.6–1.8V), optimizing power consumption. Fig. 8 presents the transient simulation results for the full access path. Enabled by minimized parasitic RC

delay, the proposed 3D DRAM achieves a nominal row cycle time ( $t_{RC}$ ) of  $<10.9$  ns (Si),  $<10.5$  ns (AOS), significantly faster than the 21.3 ns of the D1b [10] (Fig.9(c)). Disturbance-induced charge loss was analyzed via mixed-mode TCAD, assuming 10k RH toggles and  $1.5 \times 10^6$   $t_{RC}$  cycles per 64ms. Transient spikes indicate BL disturb (FBE) and WL coupling (RH). Scaling projections in Fig.9(a) show that achieving a bit density of  $2.6$  Gb/mm<sup>2</sup> requires 137 layers (height =  $9.6$   $\mu$ m) for Si and 87 layers (height =  $6.9$   $\mu$ m) for AOS. As bit density increases, Fig.9(b) illustrates the expected reduction in sense margin due to increased parasitics with FBE and RH-induced charge loss; however, the Si case maintains functional margins (70 mV) at the  $2.6$  Gb/mm<sup>2</sup> target. Energy efficiency is similarly improved; write energy is reduced to 6.26/5.38 fJ (Si/AOS), read energy to 1.57/1.35 fJ, consistently surpassing the D1b across all performance metrics (Fig.9(c)).

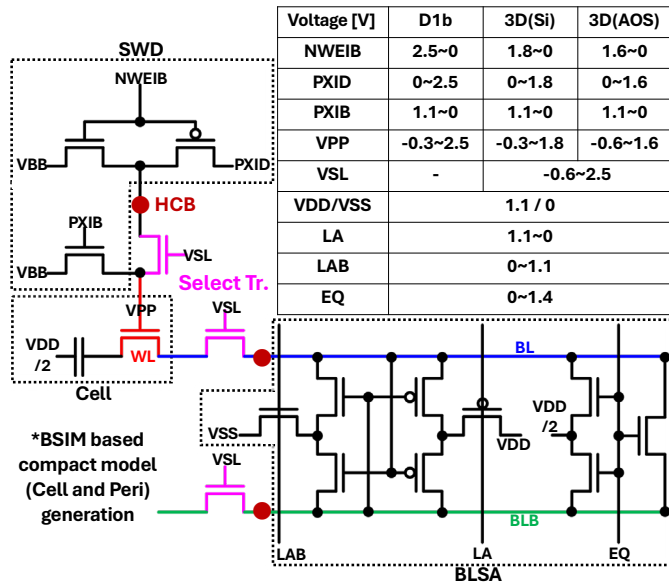


Fig. 7. Circuit diagrams utilized for SPICE simulations. The inset table summarizes the operating voltage conditions.

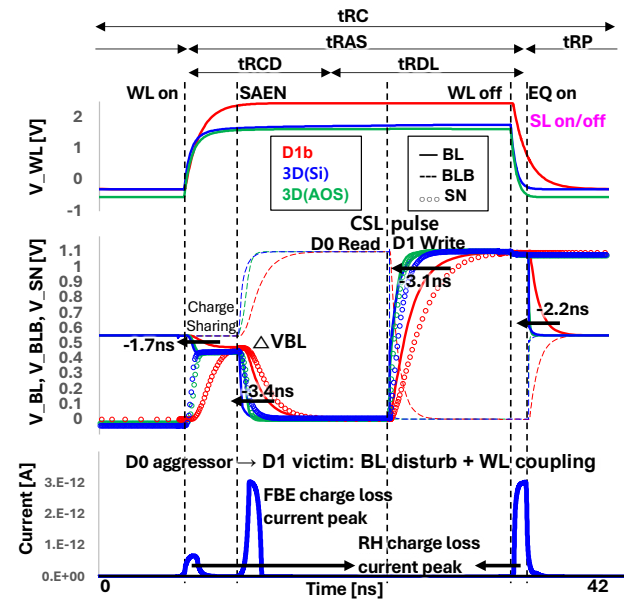


Fig. 8. SPICE/TCAD transient simulation waveforms of the full row cycle ( $t_{RC}$ , fixed 42ns, 3D DRAM  $2.6$  Gb/mm<sup>2</sup>) operation.

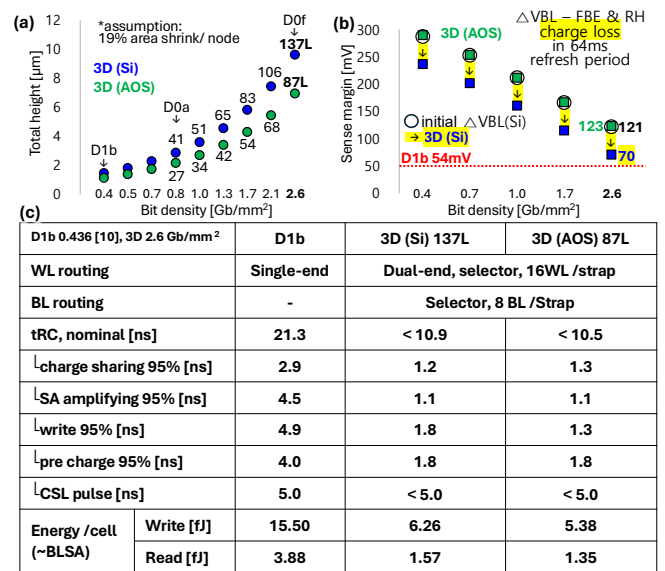


Fig. 9. Scaling projections: (a) total stack height (b) sense margin vs. bit density and (c) comprehensive comparison of architectural specifications and performance metrics (fixed  $2.6$  Gb/mm<sup>2</sup>).

### III. CONCLUSION

Our analysis confirms that the selector-strap topology effectively minimizes parasitics and vulnerability, securing robust sensing margins and manufacturable bonding pitches. 3D DRAM with CBA technology improves latency and energy efficiency over 2D baselines.

### IV. ACKNOWLEDGMENTS

This work is supported by PRISM, one of the SRC/DARPA JUMP 2.0 centers.

### REFERENCES

- [1] J. W. Han *et al.*, *VLSI*, 2023. doi: [10.23919/VLSITechnologyandCir57934.2023.10185290](https://doi.org/10.23919/VLSITechnologyandCir57934.2023.10185290)
- [2] K.S. Choi *et al.*, *VLSI*, 2024. doi: [10.1109/VLSITechnologyandCir46783.2024.10631471](https://doi.org/10.1109/VLSITechnologyandCir46783.2024.10631471)
- [3] X. Ai *et al.*, *IEDM*, 2024. doi: [10.1109/IEDM50854.2024.10873307](https://doi.org/10.1109/IEDM50854.2024.10873307)
- [4] N. Rassoul *et al.*, *VLSI*, 2025. doi: [10.23919/VLSITechnologyandCir65189.2025.11075009](https://doi.org/10.23919/VLSITechnologyandCir65189.2025.11075009)
- [5] D. Garbin *et al.*, *IEDM*, 2025. doi: [10.1109/IEDM50572.2025.11353614](https://doi.org/10.1109/IEDM50572.2025.11353614)
- [6] M. Okajima *et al.*, *IEDM*, 2025. doi: [10.1109/IEDM50572.2025.11353893](https://doi.org/10.1109/IEDM50572.2025.11353893)
- [7] K. Lee *et al.*, *TED*, 2026. doi: [10.1109/TED.2026.3659106](https://doi.org/10.1109/TED.2026.3659106)
- [8] S. Cho *et al.*, *IRPS*, 2026 (accepted). doi: <https://doi.org/10.48550/arXiv.2511.00638>
- [9] K.A. Aabarar *et al.*, *VLSI*, 2024. doi: [10.1109/VLSITechnologyandCir46783.2024.10631312](https://doi.org/10.1109/VLSITechnologyandCir46783.2024.10631312)
- [10] J. Choe, TechInsights report, 2024. [Samsung D1b DRAM Confirmed, Cell Size Much Smaller than Micron D1b](https://www.techinsights.com/reports/samsung-d1b-dram-confirmed-cell-size-much-smaller-than-micron-d1b)
- [11] E. Sarkar *et al.*, *IEDM*, 2025. doi: [10.1109/IEDM50572.2025.11353714](https://doi.org/10.1109/IEDM50572.2025.11353714)